Clinical Radiology 74 (2019) 140–149

Contents lists available at ScienceDirect

Clinical Radiology

journal homepage: www.clinicalradiologyonline.net

Texture analysis of cardiovascular magnetic resonance cine images differentiates aetiologies of left ventricular hypertrophy

R. Schofield [a,b,*,†], B. Ganeshan [c,†], M. Fontana [d], A. Nasis [e], S. Castelletti [f], S. Rosmini [a], T.A. Treibel [a,b], C. Manisty [a,b], R. Endozo [c], A. Groves [c,†], J.C. Moon [a,b,†]

[a] *Bart's Heart Centre, London, UK*
[b] *Institute of Cardiovascular Science, University College London, UK*
[c] *Institute of Nuclear Medicine, University College London, UK*
[d] *National Amyloid Centre, Royal Free Hospital, London, UK*
[e] *Monash Cardiovascular Research Centre, Monash University Department of Medicine (MMC), Melbourne, Australia*
[f] *Istituto Auxologico Italiano IRCCS, Milan, Italy*

ARTICLE INFORMATION

Article history:
Received 5 April 2018
Accepted 26 September 2018

AIM: To investigate whether unenhanced cardiovascular magnetic resonance (CMR) balanced steady state free precession (bSSFP) cine images could be analysed using textural analysis (TA) software to differentiate different aetiologies of disease causing increased myocardial wall thickness (left ventricular hypertrophy [LVH]) and indicate the severity of myocardial tissue abnormality.

MATERIALS AND METHODS: A mid short axis unenhanced cine frame of 216 patients comprising 50 cases of hypertrophic cardiomyopathy (HCM; predominantly Left ventricular outflow tract obstruction [LVOTO] subtype), 52 cases of cardiac amyloid (CA; predominantly AL: light chain subtype), 68 cases of aortic stenosis (AS), 15 hypertensive patients with LVH (HTN+LVH), and 31 healthy volunteers (HV) underwent TA of the CMR cine images (CMRTA) using TexRAD (TexRAD Ltd, Cambridge, UK). Among the HV, 16/31 were scanned twice to form a test–retest reproducibility cohort. CMRTA comprised a filtration-histogram technique to extract and quantify features using six parameters.

RESULTS: Test–retest analysis in the HV showed a medium filter (3 mm) was the most reproducible (intra-class correlation of 0.9 for kurtosis and skewness and 0.8 for mean and SD). Disease cohorts were statistically different ($p<0.001$) to HV for all parameters. Pairwise comparisons of CMRTA parameters showed kurtosis and skewness was consistently significant in ranking the degree of difference from HV (greatest to least): CA, HCM, LVH+HTN, AS ($p<0.001$). Similarly, mean, standard deviation, entropy, and mean positive pixel (MPP) were consistent in ranking degree of difference from HV: HCM, CA, AS and HTN+LVH.

CONCLUSION: Radiomic features of bSSFP CMR data sets derived using TA show promise in discriminating between the aetiologies of LVH.

* Guarantor and correspondent: R. Schofield, North West Anglia Foundation Trust, Bretton Gate, Peterborough, PE3 9GZ, UK. Tel.: +01733673817.
E-mail address: rebeccaschofield@doctors.org.uk (R. Schofield).
† Joint first authors.

https://doi.org/10.1016/j.crad.2018.09.016
0009-9260/

Abbreviations

LGE	Late gadolinium enhancement
CMR	Cardiovascular Magnetic Resonance
CMRTA	Cardiovascular Magnetic Resonance Textural Analysis
SSFP	Steady state free precession
CA	Cardiac Amyloid
AS	Aortic Stenosis
LVH	Left ventricular hypertrophy
HTN	Hypertension
HV	Healthy volunteers
AL-subtype	Amyloid light chain
LVOTO	Left ventricular outflow tract obstruction
MPP	Mean positive pixel
SD	Standard deviation
ECV	Extra-cellular volume
TA	Textural Analysis
SNR	Signal to noise ratio
CNR	Contrast to noise ratio
PSIR	Phase sensitive inversion recovery
FLASH	Fast low-angle single shot inversion recovery
FOV	Field of view
SCMR	Society of Cardiovascular Magnetic resonance
ICC	Intra-class correlation
PET	Positron Emission Tomography
SAX	Short axis stack

Introduction

The ability of cardiovascular magnetic resonance imaging (MRI) to aid in tissue characterisation has propelled its use into mainstream clinical cardiology. Late gadolinium enhancement (LGE) imaging and parametric mapping of the myocardium (native T1, T2, T2* and extracellular volume [ECV] maps) offer non-invasive assessment of myocytes and the interstitium. These techniques may require the administration of a gadolinium-based contrast agent, additional sequences, and breath-holding for the patient. They may be non-specific in early disease. The ability to mine the existing basic data set using computer algorithms is an area of current research interest. Each voxel in bSSFP data sets is an expression of the physical structure it represents.

The field of "radiomics" is the process of obtaining quantitative data from these qualitative radiological images combined with the use of artificial intelligence (AI) these data can be used to create big data sets, which can be processed and the data acquired can be linked to patient characteristics and prognostic data. With deep machine learning algorithms, this large volume dataset may be used as an ancillary diagnostic tool. Radiomics may even be used to assess response to treatment or to convey certain prognostic characteristics.

Textural analysis (TA) has been used for several decades in many domains. Within medical imaging, the technique has generated interest in diverse applications over recent years. In oncology, TA of computed tomography (CT) images has shown correlation to underlying tumour biology by differentiating different histological features (associated with the different hallmarks of cancer) and specific gene mutations.[1–4] In established malignancies, TA relates to tumour histology[5,6] across many common solid tumours (lung, colorectal, oesophageal, breast), it correlates with specific gene mutations and can track therapeutic responses.[7–10] Outside of oncology, non-malignant organ changes can be detected (for example, liver cirrhosis and usual interstitial pneumonitis).[11] TA applied to CT, MRI, and positron-emission tomography (PET) shows promise in oncological radiomics. Within cardiac imaging, TA applied to cardiovascular MRI (CMRTA) has been used to assess the risk of arrhythmia post-myocardial infarction (MI),[12] the use of CMRTA in unenhanced and LGE imaging of patients with hypertrophic cardiomyopathy (HCM) to predict outcome is a current area of particular interest.[13,14]

This project started several years ago at a time when CMRTA had not been reported. It was first hypothesised that routine CMR cine images would be amenable to TA; TA features would differentiate between the different aetiologies of disease that cause increased myocardial wall thickness (left ventricular hypertrophy [LVH]) and also healthy controls. Finally, it was hypothesised that CMRTA would provide additional supporting information, which may act as a surrogate marker for tissue abnormality by demonstrating correlation between abnormal CMRTA and the presence of LGE/increased ECV.

Materials and methods

Study population

The present study was a retrospective analysis of five cohorts of subjects. All subjects had given informed written consent for their anonymised images being used in clinical research. Analysis was performed on anonymised data from study participants who had previously provided written informed consent for CMR research approved by a local research ethics committee. The subjects comprised: (1) patients with cardiac amyloid (CA, n=52), confirmed by tissue biopsy, positive SAP scan or cardiac involvement diagnosed by echo criteria; (2) patients with HCM (n=50): randomly selected clinically confirmed HCM patients with LVH, predominantly Left ventricular outflow tract obstruction (LVOTO) subtype (recruited from an ongoing HCM study); (3) patients with severe aortic stenosis (AS, n=68) in which CMR was undertaken prior to aortic valve replacement; (4) hypertensive patients with LVH confirmed by increased indexed LV mass on echo (HTN+LVH, n=15); and

(5) healthy volunteers (HV, n=31) all prospectively recruited volunteers with no history of cardiovascular disease (normal health questionnaire, normal electrocardiogram, no cardio-active medication except for primary prevention). This group included 16 HV who were scanned twice with deliberate changes to scanning parameters to alter the signal-to-noise ratio (SNR) and contrast-to-noise ratio (CNR). This reproducibility testing was performed to identify the most robust CMRTA parameters.

CMR examination

CMR was performed using a 1.5 T clinical MRI system (Avanto, Siemens Healthcare, Erlangen, Germany) following obtained written consent for anonymised research participation. A mid short axis unenhanced balanced steady state free precession (bSSFP) cine was acquired in accordance with the Society for CMR (SCMR) guidelines as part of the routine protocol in each study.[15] The ECV was quantified. The contrast agent used was gadoterate meglumine (Dotarem, Guerbet, Paris, France) at a dosage of 0.1 mg/kg. LGE imaging was performed approximately 10 minutes following administration using either a standard fast low-angle single shot inversion recovery (FLASH) or true fast imaging with steady state free precession sequence (FISP) with a phase-sensitive inversion recovery (PSIR) reconstruction. Presence or absence of LGE was reported by an experienced CMR physician (>10 years of experience in CMR). For the amyloid cohort, T1-weighted maps and ECV quantification was performed as outlined in previous studies.[16]

In the test–retest cohort of 16 healthy volunteers, an unenhanced SSFP short axis cine was acquired in accordance to the SCMR guidelines.[15] The volunteer was taken out of the magnet and repositioned. The piloting and bSSFP short axis (SAX) cine was then repeated using a different phase-encoding direction and field of view (FOV). The studies were anonymised and randomised so the CMRTA operator was blinded. This test–retest cohort with altered imaging parameters was employed to assess the variability/reproducibility of CMRTA parameters to simulate the normal routine clinical practice where there will be variation in MRI machines and scanning protocols between different centres or between serial scans on the same magnet.

CMRTA

CMRTA was assessed using a filtration-histogram technique using a commercially available research software (TexRAD, TexRAD Ltd, www.texrad.com, part of Feedback Plc, Cambridge, UK).[3–10,17] Whole endocardial and epicardial contours were drawn identifying the whole myocardium for analysis. CMRTA comprised an initial filtration-step using a bandpass Laplacian of Gaussian filter (similar to a non-orthogonal wavelet) to extract and enhance visually imperceptible features corresponding to variation in sizes, number, and tonal intensities in relation to the background tissue/surrounding pixels defined as fine, medium, and coarse texture scales corresponding to the spatial scale filter (SSF). The SSF has typically taken the values of 2 mm (fine), 3 mm (medium), and 6 mm (coarse). This was followed by quantification of textures from the filtered intensity maps using histogram-based statistical analysis, which describes the shape of the histogram. Typical CMR SSFP imaging voxel size is 2×2×8 mm (39.6 ms repetition time [TR]/1.12 ms echo time [TE]), 55° flip angle, 192×192 matrix. Parameters included mean intensity, standard deviation (SD), entropy, mean of positive pixel (MPP), kurtosis, and skewness (Table 1).

Typically, for “normal” tissue histograms are near Gaussian, e.g., kurtosis and skewness near zero; pathology changes this.[18,19] In brief, “mean” changes approximately in proportion to the number of objects/features highlighted and their mean brightness (dark objects are negative). MPP only includes pixels greater than zero (i.e., bright) and so reduces the impact of dark objects on the mean histogram value. SD increases approximately in proportion to the square root of the number of features highlighted and their mean intensity difference compared with the background (i.e., dark and bright objects are both counted). Skewness is related to the average brightness of the highlighted features, moving away from zero with intensity variation in highlighted features and towards zero with an increasing number of features highlighted. Kurtosis is inversely related to the number of features highlighted (whether bright or dark) and increases by intensity variations in highlighted features. Entropy reflects how irregular or “random” the pixel intensity distribution is. Fig 1 illustrates the workflow of undertaking the CMRTA.

Table 1
A table outlining all the texture analysis of cardiovascular magnetic resonance imaging-derived texture parameters and their meaning.

Parameter	Definition
Mean	The average value of the pixels within the region of interest
SD	A measure of how much variation or dispersion exists from average (mean value). A low SD indicates that the data points tend to be very close to the mean; high SD indicates that the data points are spread out over a large range of values
Skewness	A measure of the asymmetry of the histogram. The skewness value can be positive or negative. A negative skew indicates that the tail on the left of the histogram is longer than the right ride. A positive skew indicates that the tail on the right side is longer than the left side. A zero value indicates the values are both evenly distributed on both sides of the mean
Kurtosis	A measure of the peakedness of the histogram. Kurtosis can be positive or negative. Positive kurtosis indicates a histogram that is more peaked than Gaussian (normal) distribution. Negative kurtosis indicates that the histogram is flatter than a Gaussian distribution
Entropy	A marker of randomness
Mean positive pixel	Considers only pixels greater than zero and so reduced the impact of dark objects on the mean histogram value.

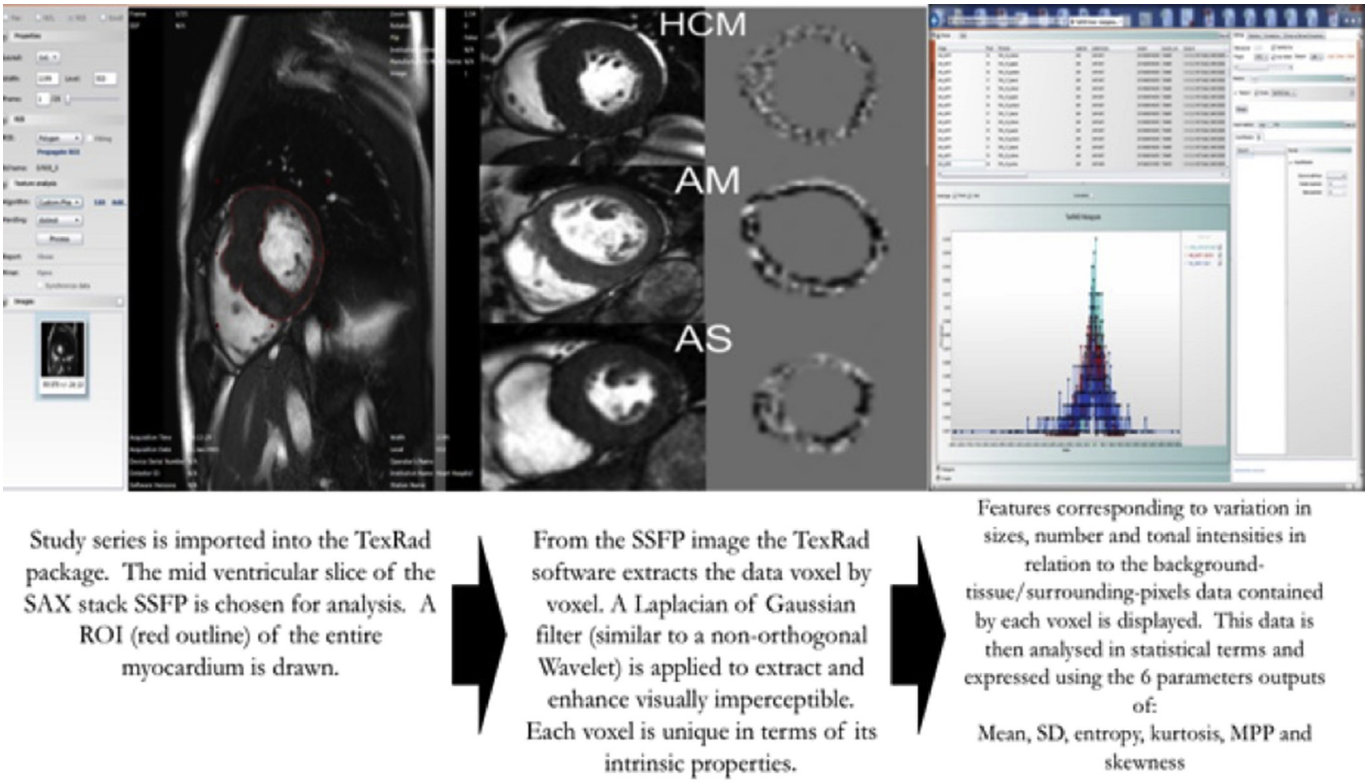

Figure 1 The TexRad histogram-filtration method of CMR image analysis workflow.

Statistical analysis

IBM SPSS Statistics (version 22, Chicago, IL, USA) was used for statistical analysis. Test–retest (reproducibility) of the CMRTA parameters across the three SSF values (fine, medium, coarse) was evaluated using the intra-class correlation (ICC). ICC >0.75 was considered to be reproducible. Bland–Altman plots were used to visualise the average-difference plot for the CMR parameters. Amongst the three different SSF values representing fine, medium, and coarse texture scales, the one that demonstrated the texture parameters to be most robust (based on the above reproducibility analyses) was further evaluated for clinical diagnostic capabilities. For each disease subtype and each preselected texture parameter, box and whisker plots were generated with non-parametric pairwise Kruskal–Wallis and Mann–Whitney tests to identify pairwise differences. Receiver operating characteristic (ROC) analysis was performed to assess the sensitivity and specificity of each parameter in differentiating AS from HTN+LVH on the basis of CMRTA alone.

The Mann–Whitney test was used to assess whether any of the derived texture parameters could differentiate between LGE positive versus negative cases. Spearman's rank correlation test was used to identify if there was a correlation between ECV and any of the derived textural parameters. A p-value of <0.001 was regarded as significant.

With five conditions, three filters, and six parameters, multiple pairwise parameters are possible to avoid issues related to multiple testing and false discovery rates, the most reproducible parameters were selected (using the test–retest reproducibility assessment in the HV as a marker of information extraction rather than scatter).

Results

Given the number of components to this preliminary study, the results are presented in the order of test–retest analysis (to inform the most reproducible filter size), Comparison of the parameters derived in HV versus all disease groups, the results of comparison between the disease states, and finally, the analysis with the disease cohorts of HCM and CA of patients with different clinical phenotypes.

Test–retest analysis

Comparing filters, the medium (spatial scale factor, SSF=3 mm) filter was the most reproducible (example: ICC for Mean, SD, skewness and kurtosis were 0.84, 0.75, 0.92 and 0.87 respectively, average ICC=0.85). Average ICC of the same parameters for fine (2 mm) was 0.70 and coarse (6 mm) was 0.76. Bland–Altman plots for mean, SD, skewness, and kurtosis using SSF=3 for the test–retest cohort is shown in Fig 2. Absolute values for the six derived parameters in HV and each disease state are shown in Table 2 (all figures to two decimal places) and Fig 3. Accordingly, only texture quantifiers at the medium filter (SSF=3 mm)

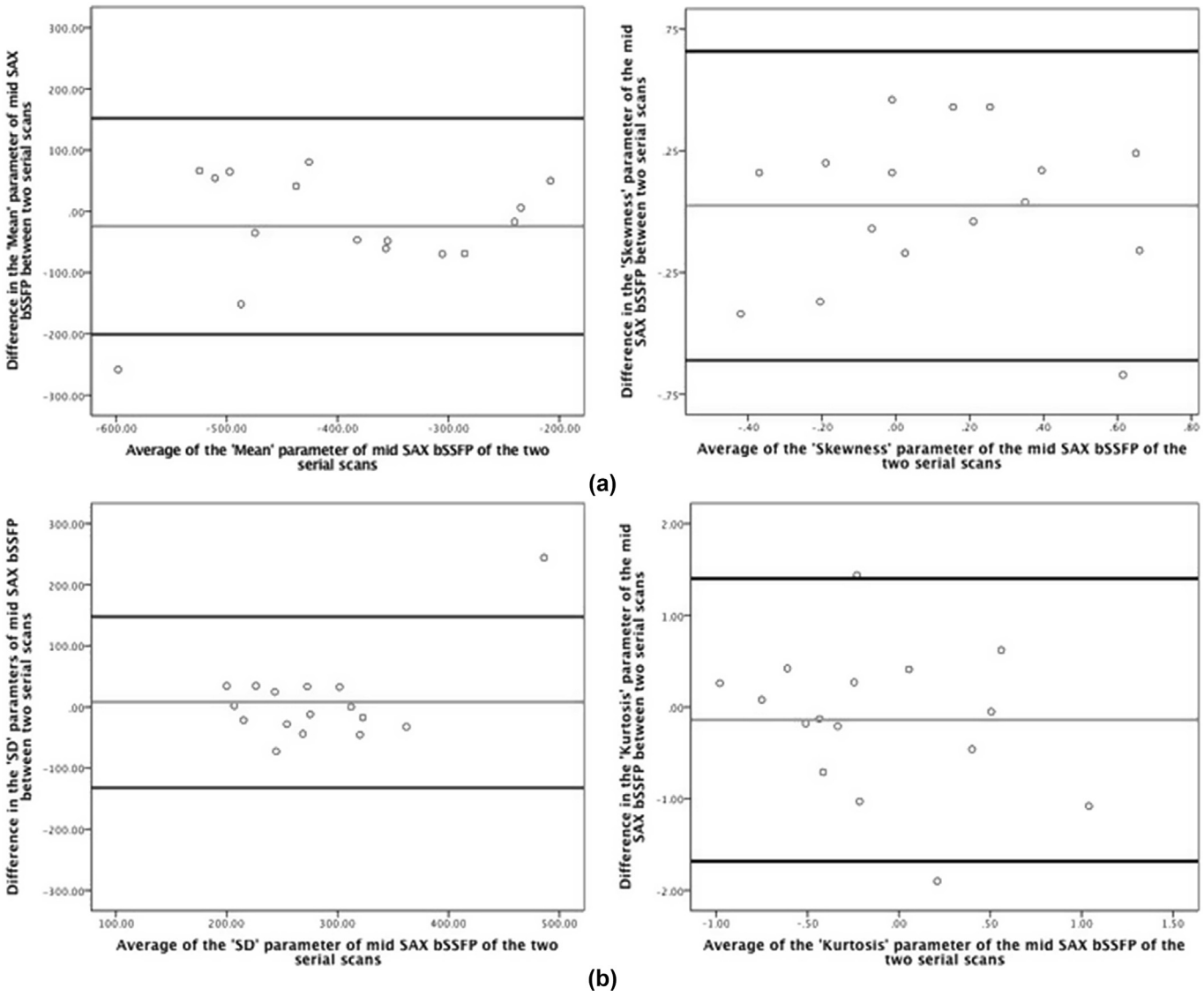

Figure 2 Bland–Altman plots for mean, SD, skewness, and kurtosis using SSF=3 for the test–retest cohort.

were pursued further for statistical analysis to evaluate clinical diagnostic capabilities.

Health versus disease (Fig 3)

Fig 3 highlights that the parameters can be positive or negative so the degree of change from zero was assessed.

Table 2
Table showing the absolute values of the six parameters for each of the disease states and healthy volunteers, using spatial filter size 3.

Parameters	HCM	Amyloid	AS	Normal
Mean	−82.48	−101.07	−211.43	−392.07
SD	105.79	144.35	199.47	273.76
Entropy	5.39	5.81	6.02	6.22
Kurtosis	2.64	3.81	1.05	−0.03
MPP	38.65	48.61	71.78	113.32
Skewness	−0.94	−1.43	−0.74	−0.00

HCM, hypertrophic cardiomyopathy; AS, aortic stenosis; SD, standard deviation; MPP, mean positive pixel.

Within the present study, mean and skewness were generally negative, suggesting more dark objects were highlighted in all cohorts, whereas SD, entropy, and MPP were generally positive. By definition SD and MPP should be positive. The fact that entropy was positive suggests a degree of irregularity within the myocardium. Kurtosis, indicates the visual contrast. A high/positive kurtosis indicates a greater range of contrast and a low/negative kurtosis indicates a narrower range of visual contrast.

Comparing the four disease states (CA, HCM, AS, HTN+LVH), to health (HV), the mean, SD, MPP, and entropy showed the greatest difference from zero in the HV whereas kurtosis and skewness were closest to zero in HV. This may suggest that in HV there is a narrower range of visual contrast and that there is a normal distribution curve of the pixel intensities in HV.

Between disease conditions, the greatest differences in parameters from HV were found for HCM (mean, SD, entropy, MPP) and CA (kurtosis, skewness). Specifically, HCM

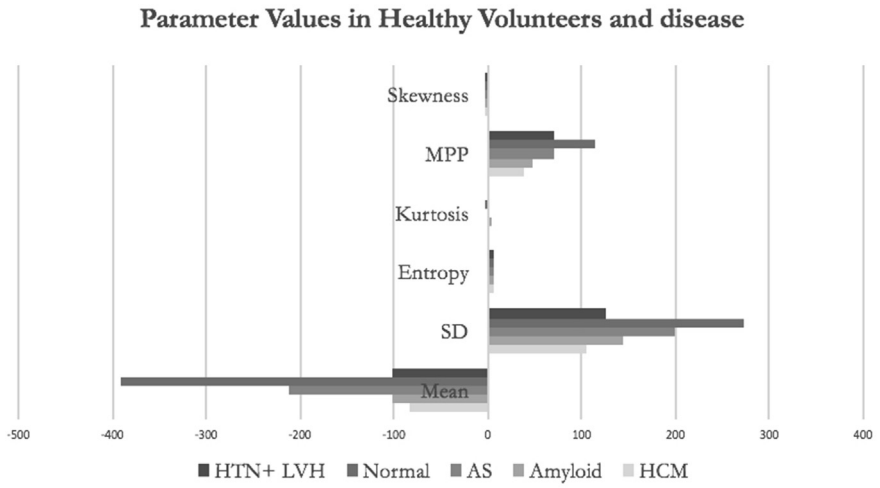

Figure 3 Bar graph showing the average values of the six parameters for each of the disease states and HV, using SSF=3.

and CA were the most different to HV (all six texture parameters statistically different, each $p<0.001$); then AS (five parameters were different $p<0.001$; entropy was not), and HTN+LVH (five were different: mean, SD, entropy, and kurtosis, each $p<0.001$, MPP $p<0.002$). The histological processes in CA and HCM differ; however, it is likely that the degree of myocardial abnormality in the CA and HCM cohorts would be greater than those in the AS and HTN+LVH cohorts. Broadly speaking, in CA there is an expansion of the myocardial interstitial matrix as a result of abnormal protein deposition. There is a predilection for subendocardial involvement; however, when compared to HCM, there is more likely to be a relatively uniform degree of abnormality compared to healthy myocardium. The finding that CA showed the largest range of pixel visual contrast (kurtosis) and skewness may suggest the detection of a "granularity" and degree of average brightness of the pixels.

Broadly speaking, in HCM there is diffuse myocardial fibrosis and myofibril disarray with patches of focal interstitial fibrosis. This would make HCM the most "random" pathology in terms of the disease pattern within the myocardium. The finding that entropy was the most different to HV, therefore, has a potential plausible explanation.

Comparing disease states: pairwise comparisons (Fig 4, Table 3).

Table 3 highlights the pairwise comparison of the study cohorts. Fig 4 demonstrates box and whisker plots for the CMRTA derived parameters across the cohorts. Within the four diseases differences (six pairs), the following results were observed:

HCM versus CA

Mean ($p=0.019$) and skewness ($p=0.002$) were negative and nearer to zero (i.e., "higher") in HCM compared to CA. SD ($p<0.001$), entropy ($p<0.001$), MPP ($p=0.002$) and kurtosis ($p=0.026$) were positive and nearer to zero (i.e., "lower") in HCM compared to CA. The pixel brightness was, therefore, higher in HCM. The pixel brightness, the number of abnormal features highlighted, and the degree of irregularity were all higher in HCM. The range of pixel visual contrast was higher in CA.

HCM versus AS

Mean ($p<0.001$) and skewness ($p=0.095$, not significant) were negative with mean being nearer to zero (i.e., "higher") whereas skewness showed a greater deviation from zero (i.e., "lower") in HCM compared to AS. SD ($p<0.001$), entropy ($p<0.001$) and MPP ($p<0.001$) were positive and nearer to zero (i.e., "lower") in HCM compared to AS. Kurtosis ($p<0.001$) was positive and away from zero (i.e., "higher") in HCM compared to AS. Therefore, compared to AS, HCM showed fewer objects highlighted but a larger range of pixel intensities and a higher degree of irregularity.

CA versus AS

Mean ($p<0.001$) and skewness ($p<0.001$) were negative with the mean being closer to zero (i.e., "higher"). Skewness, showed a greater deviation from zero (i.e., "lower") ($p<0.001$) in CA compared to AS. SD ($p<0.001$), entropy ($p=0.001$), MPP ($p<0.001$) were all positive and were nearer to zero (i.e., "lower") in CA compared to AS. Kurtosis ($p<0.001$) was also positive and more deviated from zero in CA (i.e., "higher") compared to AS. Therefore, compared to AS, CA showed fewer features highlighted but a larger range of pixel intensities and a higher degree of irregularity.

HCM versus HTN+LVH

The mean ($p=0.064$) was negative and closer to zero (i.e., "higher") in HCM compared to HTN+LVH ($p=0.064$). Skewness was also negative with a greater deviation from zero in HCM (i.e., "lower"; $p=0.001$) compared to HTN+LVH. SD ($p=0.035$), entropy ($p=0.012$) and MPP ($p<0.001$) were all positive and all were lower in HCM compared to HTN+LVH. Kurtosis showed a trend to be

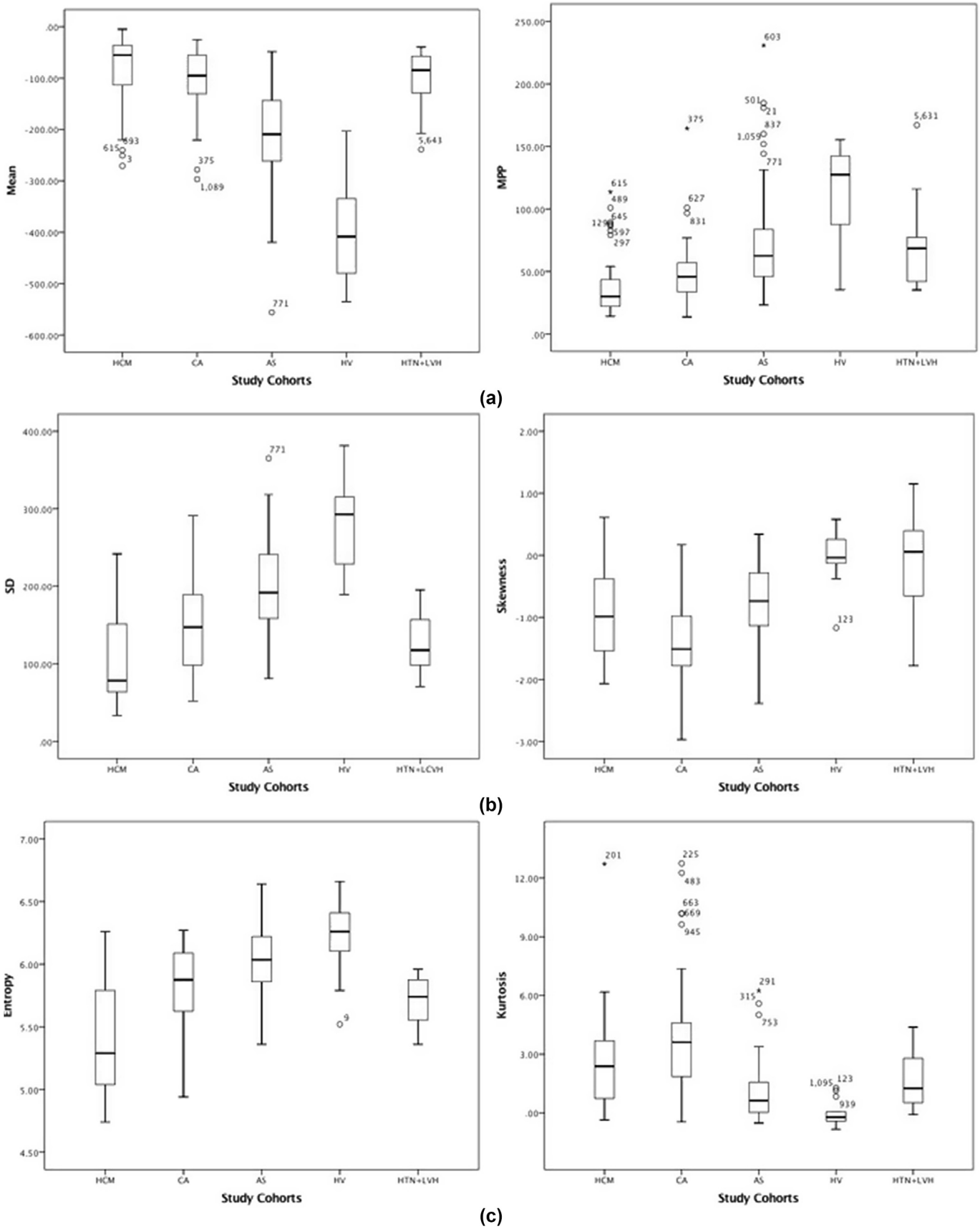

Figure 4 Using the medium scale, box and whisker plots for CMR texture parameters of mean, SD, entropy, and kurtosis across all disease types (HCM, CA, AS, HV, HTN+LVH). 0=HCM, 1=CA, 2=AS, 3=HV, 4=HTN+LVH.

Table 3
Table showing the pairwise comparison of all study cohorts and the parameters showing statistical significance.

Pairwise comparison	Parameters showing significant differences	Parameters not meeting statistical significance
HCM versus CA	SD, entropy	Mean, skewness, MPP, kurtosis
HCM versus AS	Mean, SD, MPP, entropy, kurtosis	Skewness
CA versus AS	Mean, SD, MPP, entropy, skewness, kurtosis	
HCM versus HTN+LVH	Skewness, MPP	Mean, SD, entropy, kurtosis
CA versus HTN+LVH	Skewness	Mean, SD, MPP, entropy, kurtosis
AS versus HTN+LVH	Mean, SD, entropy,	Skewness, MPP, kurtosis

HCM, hypertrophic cardiomyopathy; CA, cardiac amyloid; AS, aortic stenosis; HTN+LVH, hypertensive patients with left ventricular hypertrophy; SD, standard deviation; MPP, mean positive pixel.

higher in HCM compared to HTN+LVH, but did not reach statistical significance, (p=0.162). Interestingly, the difference between the range of pixel intensity highlighted was not statistically different between the HCM and HTN+LVH cohorts. Pixel brightness and degree of irregularity was greater in the HCM group.

CA versus HTN+LVH

The mean was negative and showed a trend to be further from zero (i.e., "lower") in CA compared to HTN+LVH, but did not reach significance (p=0.874). MPP (p=0.003) and skewness (p<0.001) were positive and significantly closer to zero (i.e., lower) in CA compared to HTN+LVH. Kurtosis was positive and higher in CA, (p=0.002). SD (p=0.198) and entropy (p=0.134) were negative and closer to zero (i.e., lower) in CA compared to HTN+LVH, but did not reach statistical significance. The degree of pixel brightness was higher in the CA cohort, but the number of features highlighted was lower. Perhaps this may explain why the entropy did not reach statistical significance.

AS versus HTN+LVH

The mean (p<0.001) and skewness (p=0.002) were negative and further from zero (i.e., "lower") in AS than HTN+LVH. SD (p<0.001) and entropy (p<0.001) were positive and further from zero (i.e., "higher") in AS compared to HTN+LVH. MPP (p=0.767) showed a trend to be lower in AS compared to HTN+LVN, but did not reach statistical significance. Kurtosis (p=0.041) was lower in AS compared to HTN+LVH. The degree of irregularity and the range of pixel intensities was higher in the AS group, perhaps suggesting more severe disruption to the myocardium (myocytes and extracellular matrix).

The strongest results could generate ROC curves, e.g., HCM (most change in parameters from HV) versus AS (least change in parameters from HV). A mean of ≥ −97.64 identified HCM from AS with a sensitivity of 72% and specificity of 94% (AUC=0.89, p<0.001, Fig 5). Kurtosis ≥1.355

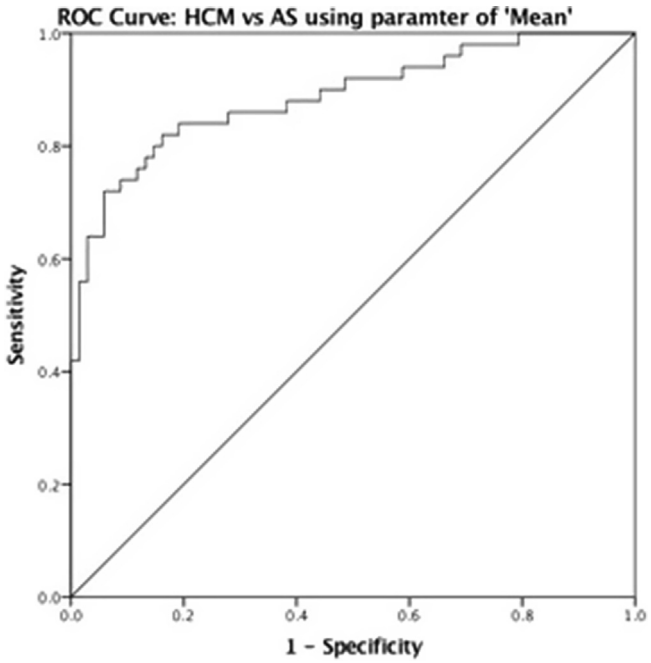

Figure 5 ROC analysis HCM versus AS using mean. A mean ≥−97.64 identified HCM from AS with a sensitivity of 72% and specificity of 94.1% (AUC=0.89, p<0.001).

identified HCM from AS with a sensitivity of 72% and specificity of 69.1% (AUC=0.75, p<0.001). An SD <158.555 identified HCM from AS with a sensitivity of 75% and specificity of 78% (AUC=0.86, p<0.001). Entropy <5.9 identified HCM from AS with a sensitivity of 72.1% and specificity of 78% (AUC=0.87, p<0.001). An MPP of <46.7600 identified HCM from AS with a sensitivity of 71% and specificity of 78% (AUC=0.81, p<0.001).

Disease subgroups: LGE in HCM and ECV in CA

Clinical phenotypic data were not collected routinely for the purposes of this preliminary study. For the disease cohorts of HCM and CA, clinical phenotypic data in the form of HCM LGE+/− and CA ECV were available. Comparison of the parameters showed that in HCM, the mean was significantly higher (p=0.031) and MPP was significantly lower (p=0.045) in LGE+ compared to LGE− group (Fig 5). For CA, the correlation between kurtosis and extracellular volume (ECV) was not significant (rs=0.222, p=0.193, n=36); however, the numbers were small.

Discussion

Within the cardiac phenotyping techniques available, imaging plays a major role, and CMR adds value because it can characterise the myocardium using techniques such as advanced LGE and parametric mapping and ECV quantification. From this preliminary study, it was found that CMR images are amenable to TA. CMRTA can differentiate between HV and disease. Specifically, HCM and CA were most different to health (all six texture parameters statistically

different, each $p<0.001$); then AS (five parameters were different $p<0.001$; entropy was not), and HTN+LVH (five were different: mean, SD, entropy, and kurtosis, each $p<0.001$, MPP $p<0.002$). CMRTA parameters showed significant differences between diseases. Specifically, mean and entropy were found in the HCM versus CA; SD, entropy, MPP, and kurtosis in HCM versus AS; skewness and MPP in HCM versus HTN+LVH; all parameters in CA versus AS; skewness in CA versus HTN+LVH and mean, SD and entropy in AS versus LVH+HTN.

It is plausible that the myocardial structure varied the most to "normal myocardium" in HCM and CA. The pattern of myocardial involvement is different between HCM and CA, and entropy reflects the degree of irregularity within the myocardium.

Further information regarding myocardial texture captured by images from standard cines may not be appreciated by the human eye, but may be detected using TA software and eventually large volume dataset machine learning could enable automated tissue characterisation. In this study, myocardial TA was most robust and richest using a medium filter (3 mm domain), which is just above pixel size. Myocardial TA may have promise in detecting differences between the causes of myocardial diseases and also for risk stratifying within a disease and assessing response to therapies. One study has shown correlation of CMRTA features to arrhythmia risk post-MI.[12]

Multiple derived parameters in newer machine-based visual-assessment techniques are challenging to rationalise. The statistical output from the filtration-histogram MRTA technique, such as mean, SD, kurtosis, skewness, MPP, and entropy, may not be intuitive to comprehend, but they are conventional descriptors for histogram distribution. With so many possible correlations, a "nested" approach was followed, starting with test–retest data to identify the most reproducible filter scale (medium texture at SSF=3 mm) followed by texture quantification at that scale to differentiate between the HV and four disease states, as well as between the disease states and with two "histological" correlations (ECV and LGE). Biologically plausible associations were found: with amyloid and HCM being much more abnormal than other diseases, a hierarchy that has credibility against known pathological differences. The CMRTA-derived parameters may provide supporting evidence of the degree of myocardial abnormality and the uniformity of that process throughout the myocardium.

Although the techniques are not refined enough currently to give a diagnosis, this area is worth exploring further. The benefits of TA are that large datasets, which are routinely acquired, can be processed, and the data acquired can be linked to patient characteristics and prognostic data. With deep machine learning algorithms, this large volume dataset may be used as an ancillary diagnostic tool or prognostic indicator. Certainly, it presents an opportunity for potential development. The benefits of this technique are that it is fast and easy to perform and does not require additional scanning time, sequences, or the administration of gadolinium-based contrast agents. It could complement more conventional imaging approaches and provide a more sensitive marker of the degree of myocardial microstructure disruption/abnormality. With the increasing use of "big data" and machine learning, it may be possible to decode these numerous statistical outputs from TA to provide a more clinically relevant and useable outcome.

In the present study, the medium texture scale was found to be robust regarding reproducibility and the texture quantifiers at medium texture scale, such as kurtosis, MPP, mean, and skewness, in particular, demonstrated diagnostic capability.

TA has been successful in the fields of oncology,[2–9,17] enabling earlier diagnosis of malignancy and as an imaging biomarker, linking imaging to genetic basis of malignancy and tracking response to treatment. In addition, various studies have shown benefit of TA in the detection of liver fibrosis with both MRI and CT.

This is a preliminary study and further research is required to fully define the role of this technique, which is rapid to perform. The strength is in the use of images that are routinely obtained without the use of intravenous gadolinium-based contrast medium. It has major potential in large-volume studies involving retrospective analysis of scans and outcome data.

Study limitations

This project, being a single-centre study with small numbers, is a pilot study. The majority of examinations were performed over several years using the same magnet. The patients in each disease cohort are likely to vary in terms of severity of disease; however, clinical phenotypic data were not recorded for the study populations. Data regarding myocardial function and patient outcome are also missing. Due to the numerous statistical comparisons, the possibility of chance findings of statistical significance is high.

The ROI used was the whole mid-ventricular section on SSFP imaging in diastole. Within a disease process, the histological features are unlikely to be uniform throughout the myocardium. CMRTA is, therefore, more suited to conditions that affect the myocardium in a diffuse and largely uniform manner. There are also limitations due to movement and blood flow. The spatial resolution of CMRTA is 1 mm. Despite this, the test–retest reproducibility cohort data were encouraging, and across all parameters, there was difference between the pathologies and HV.

In conclusion, CMRTA is a candidate clinical and research tool to describe myocardial structural disarray. It may be of patient benefit across a variety of conditions that affects the myocardium in terms of early diagnosis, prognosis, and follow-up of serial change following interventions and therapies. Further evaluation on large volume datasets from CoreLabs should be pursued.

Conflict of interest

Ethical Approval and Consent to participate- not applicable.

Analysis was performed on anonymised data from study participants who had previously provided written informed

consent for CMR research approved by a local research ethics committee at University College Hospital, London and St Bartholomew's Hospital, London, UK.

Consent for publication- not applicable.

Availability of supporting data- not applicable.

Competing interests- Dr Balaji Ganeshan is the CEO of TexRad a commercially available software used to analyze the data.

Acknowledgements

B.G. is the CEO of TexRad, the commercially available software used to analyse the data.

References

1. Kassner A, Thornhill RE. Texture analysis: a review of neurological MR imaging applications. *AJNR Am J Neuroradiol* 2010;**31**:809–16.
2. Skogen K, Ganeshan B, Good C, *et al*. Measurements of heterogeneity in gliomas on computed tomography relationship to tumour grade. *J Neurooncol* 2013;**111**:213–9.
3. Ganeshan B, Abalake S, Young RC, *et al*. Texture analysis of non-small cell lung cancer on unenhanced computed tomography: initial evidence for a relationship with tumour glucose metabolism and stage. *Cancer Imaging* 2010;**10**:137–43.
4. Sieran JC, Smith AR, Thiesse J, *et al*. Exploration of the volumetric composition of human lung cancer nodules in correlated histopathology and computed tomography. *Lung Cancer* 2011;**74**:61–8.
5. Ganeshan B, Goh V, Mandeville HC, *et al*. Non-small cell lung cancer. Histopathological correlates for textural parameters on CT. *Radiology* 2013;**266**:326–36.
6. Ganeshan B, Panayiotou E, Burnard K, *et al*. Tumour heterogeneity in non-small cell lung carcinoma assessed by CT texture analysis: a potential marker of survival. *Eur Radiol* 2012;**22**:796–802.
7. Win T, Miles KA, James SM, *et al*. Tumour heterogeneity and permeability as measured on the CT component of PET/CT predicts survival in patients with non-small cell lung cancer. *Clin Cancer Res* 2013;**19**:3591–9.
8. Ahmed A, Gibbs P, Pickles M, *et al*. Texture analysis on assessment and prediction of chemotherapy response in breast cancer. *J Magn Reson Imaging* 2013;**38**:89–101.
9. NG F, Ganeshan B, Nathan P, *et al*. Assessment of primary colorectal cancer heterogeneity by using whole-tumour texture analysis: contrast enhanced CT texture as a biomarker of 5 year survival. *Radiology* 2013;**266**:177–84.
10. Lopes R, Ayache A, Makni N, *et al*. Prostate cancer characterisation on MR images using fractal analysis. *Med Phys* 2011;**38**:83–95.
11. Depeuringe A, Chin AS, Leug AN, *et al*. Automated classification of UIP using a regional volumetric analysis in high resolution computed tomography. *Invest Radiol* 2015;**50**(4):261–7.
12. Kotu LP, Engan K, Borhani R, *et al*. Cardiac magnetic resonance image-based classification of the risk of arrhythmias in post-myocardial infarction patients. *Artif Intell Med* 2015 Jul;**64**(3):205–15.
13. Cheng S, Fang M, Cui C, *et al*. LGE-CMR-derived texture features reflect poor prognosis in hypertrophic cardiomyopathy patients with systolic dysfunction: preliminary results. *Eur Radiol* 2018 May 4.
14. Baeßler B, Mannil M, Maintz D, *et al*. Texture analysis and machine learning of non-contrast T1-weighted MR images in patients with hypertrophic cardiomyopathy—preliminary results. *Eur J Radiol* 2018 May;**102**:61–7.
15. Kramer CM, Barkhausen J, Flamm SD, *et al*. Standardized cardiovascular magnetic resonance imaging (CMR) protocols, society for cardiovascular magnetic resonance: board of trustees task force on standardized protocols. *J Cardiovasc Magn Reson* 2008;**10**:35. https://doi.org/10.1186/1532-429X-10-35.
16. Fontana M, White SK, Banypersad SM, *et al*. Comparison of T1 mapping techniques for ECV quantification. Histological validation and reproducibility of ShMOLLI versus multibreath-hold T1 quantification equilibrium contrast CMR. *J Cardiovasc Magn Reson* 2012;**14**:88.
17. Ozkan E, West A, Dedelow JA, *et al*. CT gray-level texture analysis as a quantitative imaging biomarker of Epidermal Growth Factor Recptor mutation status in adenocarcinoma of the lung. *AJR Am J Roentgenol* 2015;**205**:1016–25.
18. Miles KA, Ganeshan B, Hayball MP. CT textural analysis using the filtration-histogram method: what do the measurements mean? *Cancer Imaging* 2013;**13**:400–6.
19. Sala E, Mema E, Himoto Y, *et al*. Unravelling tumour heterogeneity using next-generation imaging: radiomics, radiogenomics, and habit imaging. *Clin Radiol* 2017;**72**:3–10.